

## Diurnal Climatology of the Boundary Layer in Southern California Using AMDAR Temperature and Wind Profiles

DAVID A. RAHN AND CHRISTOPHER J. MITCHELL

*Department of Geography and Atmospheric Science, University of Kansas, Lawrence, Kansas*

(Manuscript received 27 August 2015, in final form 9 March 2016)

### ABSTRACT

Observations from commercial aircraft [e.g., the Aircraft Meteorological Data Relay (AMDAR) automated weather reports] have been increasing dramatically. Two main applications of the aircraft data are use in short-term forecasts and assimilation into numerical weather prediction models. Now that more than 10 years of measurements exist, using this dataset to construct a description of the long-term climatological behavior (a “climatology”) of the lower atmosphere is explored with two main objectives. The first objective is to examine strengths and weaknesses of using the dataset to construct a climatology of the lower atmosphere. Unlike the traditional twice-daily radiosonde launches, the high frequency of observations at major airports allows for an unprecedented set of diurnal information at many locations globally. The second objective is to obtain a climatology of the lower atmosphere of Southern California, specifically at Los Angeles, San Diego, and Ontario, during the spring and summer when the boundary layer is well defined and easily detected. The June 2001–14 climatology reveals that the deepening of the boundary layer overnight is consistent with a cloud-topped boundary layer. Whereas the average boundary layer height decreases right after sunrise at San Diego, at Los Angeles the deeper boundary layer persists about 4 h after sunrise and then decreases rapidly over 2 h as the onshore sea breeze strengthens. Morning intrusions of the marine air inland are easily detected at Ontario in some months but are practically nonexistent during July and August.

### 1. Introduction

Observations of the profile of temperature, moisture, and wind are critical for knowing the current state of the atmosphere, short-term forecasting, assimilating into numerical models, and understanding the climate. Vertical temperature profiles are particularly important for high-impact events such as forecasting severe weather, fog, or the dispersion of air pollution. In coastal upwelling zones like the western coast of the United States, there is often a shallow marine atmospheric boundary layer that can be difficult to simulate and forecast correctly ([Angevine et al. 2012](#)). Coastal fog and low stratus associated with the marine layer greatly affect air travel by causing airport closures. The refractivity structure of the lower atmosphere influences the propagation of electromagnetic radiation and has consequences for radar detection systems, which is a national security issue (e.g.,

[Burk and Thompson 1997; Brooks et al. 1999; Haack and Burk 2001; Wang et al. 2012](#)).

Radiosondes, which are typically launched up to 2 times per day (0000 and 1200 UTC) across the globe, do not contain adequate information to capture the entire diurnal cycle. More frequent measurements of the lower atmosphere have been obtained through dedicated field campaigns that launch radiosondes or use aircraft (e.g., [Blaskovic et al. 1991; Rogers et al. 1998; Angevine et al. 2012; Rahn et al. 2013](#), and many others), but these are typically conducted over a short period and at limited locations. The National Oceanic and Atmospheric Administration (NOAA) Profiler Network provided high-frequency wind measurements but was terminated in 2014, in part because of the increasing availability of high-quality reports from commercial aircraft at lower costs ([NOAA 2014](#)).

The value of measurements from commercial aircraft is becoming more widely recognized. The Aircraft Meteorological Data Relay (AMDAR) automated weather reports are reported in real time over the Aircraft Communication Addressing and Reporting System (ACARS), which includes all aircraft data. The number of commercial

*Corresponding author address:* David A. Rahn, Dept. of Geography and Atmospheric Science, University of Kansas, 201 Lindley Hall, 1475 Jayhawk Blvd., Lawrence, KS 66045-7613.  
E-mail: darahn@ku.edu

aircraft providing AMDAR reports has continued to increase greatly. As of July 2013, commercial aircraft provide over 400 000 point observations per day on average and come from 39 participating airlines, according to the World Meteorological Organization (WMO 2014b). Observations are expected to keep growing partly because the National Weather Service plans to use part of the Disaster Relief Appropriations Act of 2013 to expand coverage (NOAA 2014). Aircraft measurements are most frequently used to improve short-term forecasts and to improve numerical weather prediction by assimilating them into the analysis field for better initial conditions, but they have seldom been used for climatological studies (e.g., Cardinali et al. 2003; Gao et al. 2012; Petersen 2016). After more than a decade of observations, these data can potentially be a great asset to the operational and research community because they can be used to characterize the lower atmosphere at such a high temporal resolution near major airports. A major advantage of AMDAR over the operational radiosondes is that AMDAR observations can be obtained during much of the day. Furthermore, multiple measurements may be obtained in the vicinity of each other and near the same time, leading to large sample sizes near busy airports.

Many meteorological processes are tied to the atmospheric boundary layer. Field studies, operational radiosondes, and theory have provided a better understanding of the boundary layer, but a lack of standard observations at all hours of the day in the lower atmosphere has inhibited some areas of progress. Observations of the boundary layer/lower atmosphere are still needed for many basic research questions. Without long-term data, systematic biases in simulations cannot be identified. One of the largest uncertainties is the nocturnal boundary layer (e.g., LeMone et al. 2014). A recent field campaign is the Plains Elevated Convection at Night (PECAN), which is examining elevated convection at night. As part of that field campaign, many soundings were launched to observe the lowest part of the atmosphere at night, which is not represented well in numerical models. Representation of the boundary layer has improved in numerical weather simulations, but parameterizations of boundary layer processes are by no means perfect. Much effort is still being made to evaluate and improve this aspect of the models (e.g., Angevine et al. 2012). In Hu et al. (2010), a set of simulations using different planetary boundary layer schemes was run over Texas from July through September 2005. This output was compared with AMDAR measurements in the Dallas–Fort Worth (Texas) area to evaluate these schemes over this period.

AMDAR can now be used to systematically characterize the lower atmosphere at locations and times other than the traditional operational radiosonde launches at

0000 and 1200 UTC. Some applications of this extremely valuable dataset of in situ observations are explored here, and this dataset may be used to great effect on a broad range of questions. In addition to evaluating the strengths and weaknesses of using AMDAR data for creating a description of the long-term climatological behavior (a “climatology”) of the lower atmosphere, variations in the diurnal climatology of the boundary layer at several sites in Southern California are presented. Southern California is selected for several reasons, including the high volume of data and the existence of a well-defined boundary layer during the spring and summer. The depth of the boundary layer and characteristics of the lower atmosphere are key components for issues such as episodes of high air pollution, visibility conditions at the coastal airports, and phenomena such as Catalina eddies. Catalina eddies represent an enhanced cyclonic circulation in the California Bight and are known for their extensive low stratus coverage along the eastern half of the California Bight, often deepening near the coast and extending inland through mountain passes. Since publication of the satellite image by Rosenthal (1968), Catalina eddies have attracted considerable attention (Bosart 1983; Wakimoto 1987; Mass and Albright 1989).

There are two main objectives of this work. The first objective is to provide some detail and illuminate issues with constructing a climatology of the lower atmosphere using AMDAR. The second objective is to apply the dataset to obtain a diurnal climatology of the lower atmosphere in Southern California that can be used as a baseline for investigating anomalies from the base state such as strong Catalina-eddy events. Although only 10 years of substantial data are currently available, future studies can examine longer-term changes to the lower atmosphere.

Details of the dataset and processing methods are described in the next section. This is followed by an application of the constructed climatology of specific features related to the boundary layer in Southern California, specifically at San Diego, Los Angeles, and Ontario. The final section summarizes the strengths and weaknesses of using AMDAR, as well as the results of the climatology of Southern California.

## 2. Data and methods

### a. AMDAR

Aircraft observations date back to World War I and were the primary source of upper-air measurements during that time. With the development of the radiosonde and the first official launch in 1937, the 30 regularly scheduled flights per day were eventually replaced by the weather balloon. It was not until 1979 when automated

aircraft reports became available that the amount of aircraft data began to modestly increase. The quality of the data was good, but the system was still not suitable for real-time applications, and measurements were sparse (Lord et al. 1984). In the mid-1990s the number of aircraft that reported meteorological information began to increase rapidly. As of July 2013, the World Meteorological Organization (WMO 2014b) reported that there are 39 participating airlines that contribute  $\sim 400\,000$  daily observations (single point measurements made by all aircraft in space and time), and that number is expected to keep increasing. Because of the variety of international programs that were involved with the reemergence of aircraft data, several different systems and labels are used to refer to those data (Moninger et al. 2003).

Reports from the current fleet of aircraft equipped with meteorological instruments have at least temperature and horizontal wind. In more recent times, a greater number of aircraft also carry instruments that measure water vapor and turbulence. When AMDAR observations were compared with radiosonde measurements, a systematic warm bias of the AMDAR data was found (Ballish and Kumar 2008). The magnitude of the warm bias varied with height such that near the surface it was a few tenths of a degree but at higher altitudes it increased up to  $1^{\circ}\text{C}$ . This bias is recognized by several of the numerical weather prediction centers, and steps have been taken to address it during the data-assimilation step (e.g., Isaksen et al. 2011; Zhu et al. 2015). Because this study is examining the lower atmosphere, the warm bias is small. In addition, identification of the boundary layer depth is unaffected by a bias because it is the relative change of temperature with height that is used to identify the top of the boundary layer.

Data from AMDAR are available in real time to users with consent from the participating airlines. Archived data older than 48 h are available publicly and can be found on the Meteorological Assimilation Data Ingest System (MADIS) in the Network Common Data Form (NetCDF) under the classification of ACARS data ([https://madis.noaa.gov/madis\\_acars.shtml](https://madis.noaa.gov/madis_acars.shtml)). These NetCDF files are archived hourly, resulting in 24 individual files per day, splitting many soundings between files. Measurements are provided in two formats. The first format is all of the raw data reported as individual point measurements. The second format is profile data, in which data during level flight are removed.

Soundings here are created using the hourly raw data files that are available from the URL given above. Because the total disk space of all 2001–14 uncompressed hourly files is 1.3 terabytes and the region of interest is only the lower atmosphere of Southern California, a subset of the data over the region and below 3 km was created before extracting the

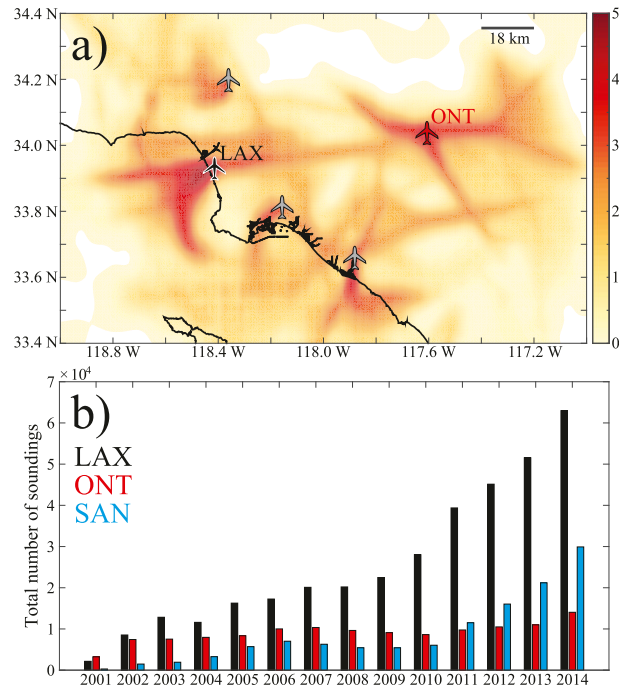


FIG. 1. (a) Density plot of the log of all AMDAR point observations (2001–14) in  $0.01^{\circ} \times 0.01^{\circ}$  bins under 3 km in the Los Angeles basin. (b) Total number of soundings per year (units of 10 000) at each airport.

soundings. Point observations were sorted by aircraft tail number and grouped into consecutive measurements with time gaps of no larger than 2 min. In addition, to qualify as a sounding, there must be at least 10 observations and at least 1 observation within 200 m of the surface. Because there are several airports in the vicinity of each other in the Los Angeles basin (Fig. 1a), each sounding was identified with an airport by taking the lowest observation and checking if it was within 15 km of an airport. Other criteria can be used, and the choice is ultimately dictated by the particular application.

#### b. Spatial and temporal distribution of soundings

In the Los Angeles basin there are several airports within approximately 100 km of each other (Fig. 1a). Between 2001 and 2014, Los Angeles International Airport (LAX) had the highest AMDAR traffic while Ontario International Airport (ONT) had the second highest traffic, with 346 439 and 128 790 total soundings, respectively. Farther to the south, San Diego International Airport (SAN) had 118 303 total soundings. The flight corridors of the arriving and departing aircraft are evident in the log of the density plot of all point observations. Most of the aircraft observations near LAX were taken over the ocean because of noise-abatement policies, and therefore the results shown here reflect a marine environment.

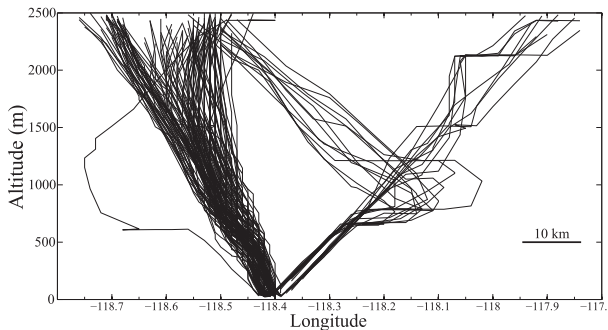


FIG. 2. Longitudinal profiles of flights at LAX on 6 Jun 2013. Flight approaches and departures were from east to west on this day.

A longitude–altitude plot of the flight tracks over one day (Fig. 2) depicts the preferred flight path to the west and also illustrates the typical horizontal displacement of the observations from the airport with height. Radiosonde observations are more vertical than aircraft observations. Given that the target ascent rate for a radiosonde is  $275\text{--}350 \text{ m min}^{-1}$  (about  $5 \text{ m s}^{-1}$ ) and given a horizontal wind of  $\sim 5 \text{ m s}^{-1}$ , the horizontal displacement from the launch site would be 1 km at an altitude of 1 km. For a typical flight path (Fig. 2), the horizontal displacement from the airport is about 10 km at a height of 1 km. In situations in which the atmosphere is roughly homogeneous, significant differences in the vertical profile as a result of horizontal displacement are unlikely, but in areas with larger horizontal gradients, such as near the coast, there could be substantial differences in the vertical profile. This issue will be revisited when examining soundings at SAN. Furthermore, there could be issues that are due to differences in ascending or descending flight paths. Profiles were separated into those associated with ascent and those associated with descent, and results were qualitatively similar.

At LAX and SAN there has been a pronounced increase in the total number of soundings since 2001 (Fig. 1b). LAX had  $\sim 10\,000$  soundings in 2002 and over 60 000 soundings in 2014. At ONT the number of soundings has remained around 10 000 per year. The reason why ONT has remained steady is because it is one of the hubs of the United Parcel Service (UPS), which was one of the early adopters of the system. The MADIS archive begins in July 2001, and therefore the analysis of the subsequent daily averages will only consider the period of 2002–14, which has full years. A 1-h interval is used to bin the observations. Longer intervals increase the sample size in each bin but reduce the sharpness.

Unlike the regular radiosonde launches at 0000 and 1200 UTC, the sampling by the aircraft is not uniformly distributed over the course of the day, which could be a problem for the analysis. In addition, sampling at each

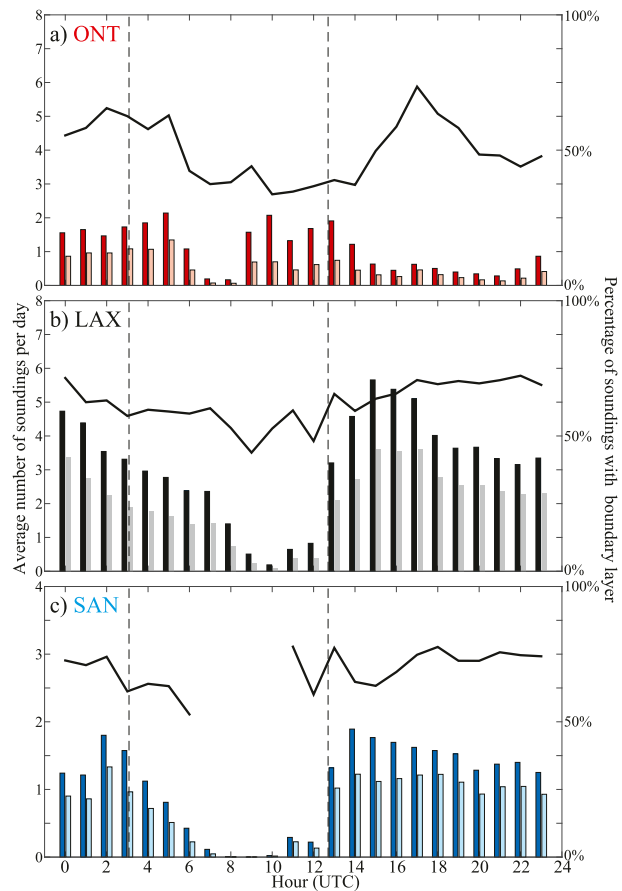


FIG. 3. For 2002–14, the average number of total soundings (dark bar) and soundings with a detected boundary layer (light bar) each hour per day for (a) ONT, (b) LAX, and (c) SAN (note the different scales). The solid black line is the fraction of soundings with a detected boundary layer. As a reference, the vertical dashed bars indicate the sunrise and sunset on 15 June.

airport can be different. At major transportation hubs there are typically fewer passenger flights that land or take off late at night and before dawn (Fig. 3). This may be an issue for obtaining good diurnal statistics of meteorological variables. On the other hand, ONT has the most flights in the evening and early morning hours because it is a hub for UPS, which ships air cargo overnight. During the off-peak hours at LAX, there is only about one sounding every other day. In contrast, during peak travel times there is an average of six soundings per hour. Depending on the application (e.g., examining the evolution of the boundary layer during Catalina eddies or studying landfalling synoptic systems, high-pollution periods, etc.), different strategies could be employed to handle the irregular distribution of data.

Although LAX and ONT have fewer soundings during off-peak hours, SAN has a time gap in data from 0700 through 1000 UTC. This lack of data presents one

obvious challenge to constructing a diurnal cycle of the lower atmosphere. Even at fairly busy airports there can be missing data over certain time periods. Despite this 4-h period, the information from the other times of the day is valuable and useful, as will be shown.

The vertical sampling interval by each aircraft is variable and has evolved over time (WMO 2014a; Petersen 2016). During level flight, observations are taken approximately every 5 min. While arriving at or departing from the airport, there is a measurement about every 90 m. To produce a uniform grid, all soundings are linearly interpolated to a regular height located at every 20 m. The 20-m interpolation is a relatively fine resolution when compared with the average sampling, which is at best  $\sim 100$  m, but is done in part to capture the observations that are near the surface. For instance, for a coastal airport with an elevation near sea level, the first observations could be 20 m off the ground. Thus, information near the surface would be lost if the heights for interpolation were every 100 m.

### c. Determination of the height

For this analysis, it was preferable to use height above the ground as the vertical coordinate. Using pressure would have broadened the distribution because surface pressure changes on diurnal, synoptic, and seasonal time scales. The vertical position of the aircraft in the archived data is given as the pressure altitude. The pressure altitude is determined from the measured static pressure using a standard atmosphere. Thus, the pressure altitude is really just a pressure measurement. This is an important detail to recognize because users who are not careful may at first confuse the pressure altitude with an actual altitude. The pressure altitude can depart greatly from the actual height above sea level and even be “below ground” if the difference between the actual and standard pressure is large. We emphasize that a pressure altitude that is below ground is *not* an error and that data should not be thrown out in some misguided effort of quality control. It is natural that sometimes the pressure altitude is below ground because, again, the pressure altitude is really just a pressure measurement.

To obtain an estimate of the true height of each sounding, the pressure altitude and standard atmosphere were used to recover the original static pressure measurement. Then the nearest hourly observation of pressure and temperature from the surface meteorological station at the corresponding airport was obtained. The pressure observations at the airport meteorological stations have a high degree of accuracy and reliability because pilots need these reports to set their altimeter. The final height is found by integrating the hypsometric equation from the surface upward using the recovered static pressure and temperature

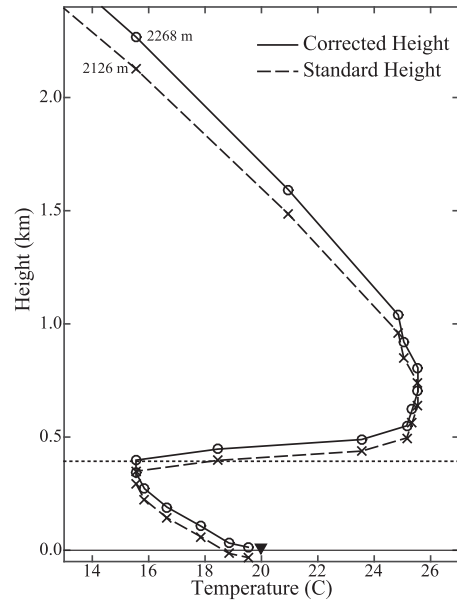


FIG. 4. Temperature profile from SAN at 1600 UTC 20 Jun 2007 using the height obtained with the standard atmosphere (dashed line) and the corrected height described in the text (solid line). The markers on each line are the discrete measurements. The dashed line indicates the height of the boundary layer found by the objective algorithm. The solid triangle is the temperature from the surface station.

measurements from the aircraft and the surface pressure, temperature, and station elevation.

During June in Southern California, the differences between the height using the standard atmosphere and actual temperature and pressure are often small for many soundings. Even during this relatively quiescent period there can be large departures in height, however. An example of the difference is given in Fig. 4, which shows a sounding from SAN at 1600 UTC 20 June 2007. At the lowest level the pressure altitude is  $-31$  m (below ground) while the corrected height is 15 m, a difference of 46 m. Errors accumulate as the hypsometric equation is integrated upward such that near 2 km above the surface the standard atmosphere height is 2126 m while the corrected height is 2268 m, a difference of 142 m.

Although the example at SAN is one of the larger differences during June, there can be much larger departures at other times of years and at other locations. For example, if the center of a strong cyclone or anticyclone passes near an airport, extremely large errors will occur and will greatly skew the results. It is extremely important to make this correction when using AMDAR data.

### d. Definition of the boundary layer used in this study

Information on the depth of the boundary layer is a critical parameter for a variety of applications from

studying the concentration of air pollutants to understanding the regional dynamics. The boundary layer depth is defined here as the height of the minimum temperature at the base of the strongest temperature inversion. This is similar to other marine boundary layer studies (e.g., de Szoëke et al. 2012). No boundary layer depth is reported if there is no temperature inversion, if the temperature inversion is too weak ( $<2\text{ K km}^{-1}$  over a 60-m layer), or if the temperature inversion extends to the bottom of the sounding, which commonly occurs when there is a surface radiation inversion. The percentages of soundings that have an identifiable boundary layer are shown in Fig. 3. LAX and SAN are fairly consistent at about 62% and 70%, respectively, throughout the day. Overall, ONT averages 50%, but there is a clear diurnal difference such that soundings have a lower percentage of detected boundary layer heights in the morning (~35%) as opposed to the middle of the day (~75%). The low percentages during the night and morning are often due to the presence of a surface radiation inversion at this inland location and a weak residual boundary layer aloft.

During the spring and summer the cool marine boundary layer along the coast of California is normally capped by a marked temperature inversion that is associated with large-scale subsidence. Thus, the boundary layer is often well defined during the warm season so that the algorithm can unambiguously identify the base of a single, major temperature inversion. This is not the case during the autumn and winter when the large-scale subsidence relaxes and the marine boundary layer is disturbed more often by synoptic intrusions such that no clear well-mixed layer capped by a temperature inversion is detected by the algorithm. The seasonal difference is exemplified by comparing LAX in June versus November (Fig. 5). A clear boundary layer depth is found in 88% of the soundings during June but in only 43% during November. Failure to detect a boundary layer height occurs when the temperature inversion extends down to near the surface so that no inversion base is detected, no inversion even exists, or the inversion is too weak.

### 3. Results

Three major airports in Southern California (LAX, ONT, and SAN) are initially considered separately. Much of the analysis will focus on June because that is when the boundary layer is most robustly present, but a summary of other months is also provided. At the end of this section, the results from these three airports are compared with each other to describe the climatology of the lower atmosphere in the region during June.

Much effort has been made to understand the role of clouds in the marine boundary layer on the diurnal cycle

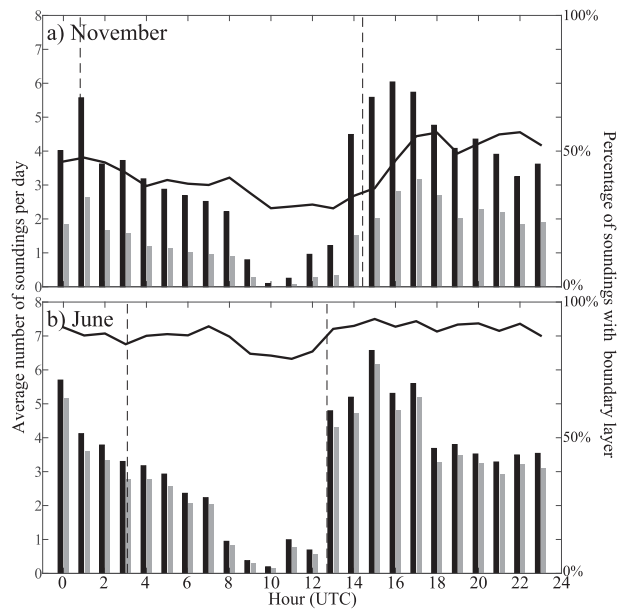


FIG. 5. As in Fig. 3, but at LAX for (a) November and (b) June.

using modeling studies and observations (e.g., Lilly 1968; Stevens et al. 2003, and many others). In addition to the climatology using all times, conditional subsets have been created to separate the diurnal cycle on the basis of the condition of cloudy or clear using surface observations of clouds with bases below 2 km since it is boundary layer clouds that are the most pertinent. Because the impact of the clouds on the boundary layer is an integrated effect, the average octas of the low-level clouds of the current and previous 2 h of observations were used. A sounding is classified as cloudy if the average octas were at least four and clear otherwise. Use of other criteria such as fewer than three and more than five for clear and cloudy, respectively, produced similar results but smaller sample sizes.

#### a. LAX

Ample soundings with a well-defined boundary layer height are available at LAX for most hours (Fig. 6). For reference, 2000 soundings in an hourly bin correspond to approximately 5 soundings per day. The exception is at 1000 UTC when there are only 61 soundings in June over the 14-yr period. The analysis begins with all soundings to present the general climatology, and then the climatology is conditioned on clear and cloudy days, which likely are the dominant control on the boundary layer. As a result, the general climatology is an out-of-focus merger of these two distinct states. Boxplots indicate that the distribution of boundary layer height for all sky conditions is close to normally distributed but is skewed slightly toward

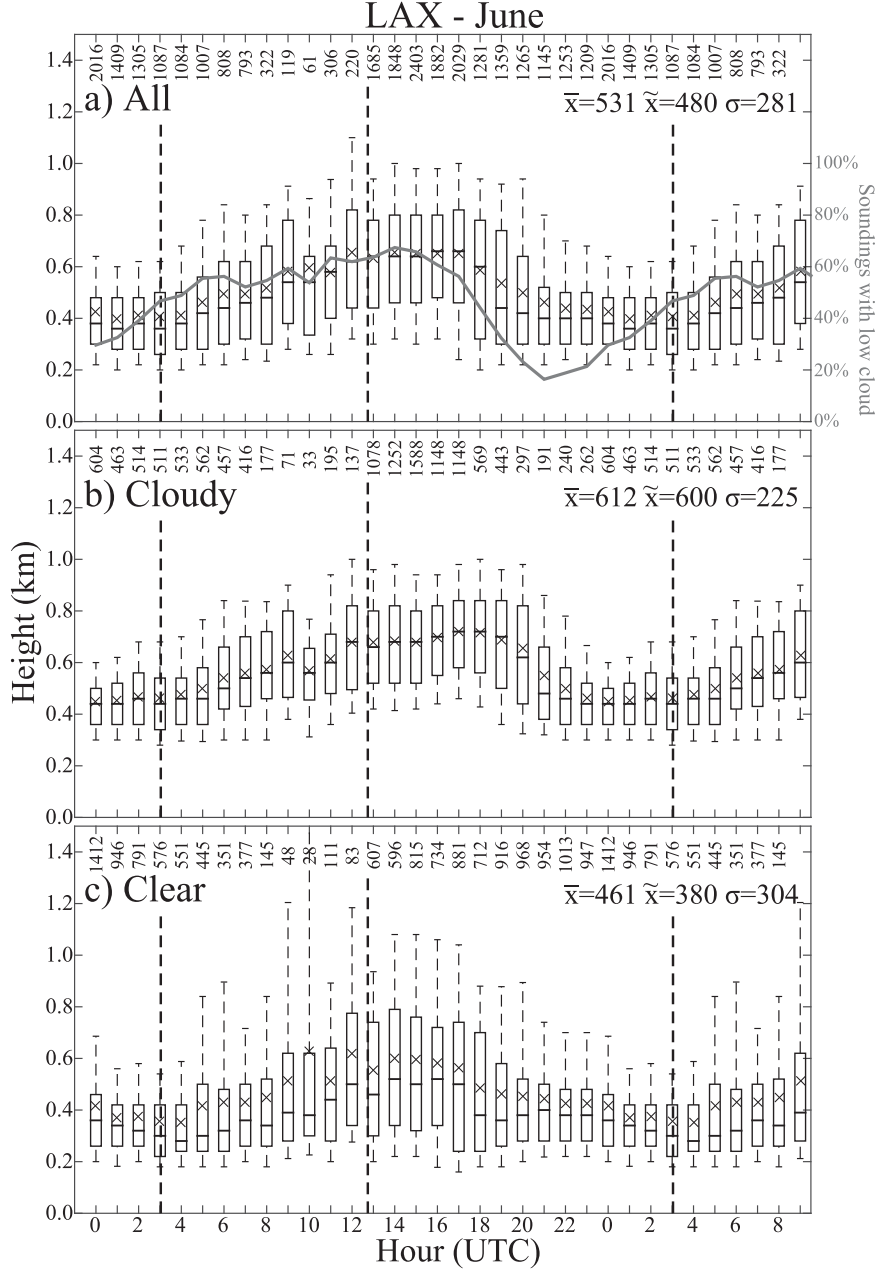


FIG. 6. Boxplot of boundary layer depth (km) at LAX for June 2002–14 for (a) all soundings, including the percent of soundings with low cloud (gray line), (b) cloudy conditions, and (c) clear conditions. The median is the horizontal line, the mean is the x, the box contains the interquartile range, and the whiskers extend to the 10th and 90th percentiles. The numbers at the top of (a)–(c) indicate the total number of soundings included in each hourly bin. The vertical dashed bars indicate the sunrise and sunset on 15 June. Summary statistics for the full dataset, including the mean  $\bar{x}$ , median  $\tilde{x}$ , and standard deviation  $\sigma$  of MBL height are given in (a)–(c).

higher heights. The diurnal cycle of the average boundary layer height is evident. Shortly after sunset, the boundary layer deepens at a rate of about  $25 \text{ m h}^{-1}$  throughout the night and into the morning, at which time the depth remains fairly steady until decreasing

rapidly at 1800 UTC and then more slowly in the hours leading up to sunset (0300 UTC). Just before sunset the interquartile range is the smallest, indicating a fairly regular range of boundary layer height at this time. The largest interquartile range occurs when the

boundary layer height decreases, which is likely a reflection of the different timing of the initial decrease on different days.

Dividing the observations of boundary layer depth into cloudy and clear (Figs. 6b,c), the differences in the distribution and diurnal cycle become more notable. When there are low-level clouds (presumably boundary layer clouds), the shape of the diurnal signal is similar to the average using all soundings. This result attests to the dominance of boundary layer clouds overnight and into the morning in June. In the morning at 1300 UTC, 64% (36%) of the time it is cloudy (clear). In the afternoon at 0000 UTC, 70% (30%) of the time it is cloudy (clear). The boundary layer is deeper under cloudy conditions, with an average difference of 105 m (175 m) in the mean (median). The deep boundary layer present on cloudy mornings persisted longer into the day, with boundary layer depths decreasing after 2000 UTC, which is several hours after the average of all soundings. The persistence of the deep boundary layer points to the difference in the diurnal cycle from a coastal boundary layer to an offshore cloud-topped marine boundary layer. The diurnal cycle of an offshore cloud-topped marine boundary layer is characterized by the greatest depth occurring right after sunrise and decreasing shortly after the sun comes up. Even though clouds play a major role both near shore and offshore, other factors must also contribute to the diurnal cycle near the coast. Furthermore, the standard 0000 and 1200 UTC climatologies cannot pick up this lagged peak.

Under clear-sky conditions, diurnal boundary layer variations are less well organized, with large interquartile ranges during the morning and a peak in the mean and median that occurs around 1500 UTC. Part of the ambiguity in the signal may be due to the definition of cloudy versus clear conditions. Because the surface observations at the coast are used, this method does not account for upstream conditions that may be cloudy. To summarize the daily boundary layer depth at LAX, the average of the mean and standard deviation of boundary layer depth at each hour was calculated for all, cloudy, and clear conditions. For all soundings, the average boundary layer depth is 527 m, with a standard deviation of 267 m. For cloudy soundings, the average boundary layer depth is 583 m, with a standard deviation of 199 m. For clear soundings, the average boundary layer depth is 478 m, with a standard deviation of 316 m. In addition, summary statistics of the boundary layer depth using all data are included in each panel of Fig. 6 for reference.

Although June is the focus of this climatology, the average diurnal cycle during the warm season (May–October) illustrates the month-to-month variation at LAX (Fig. 7a). There is a fairly clean break in the diurnal cycle between the warmest months of July–September

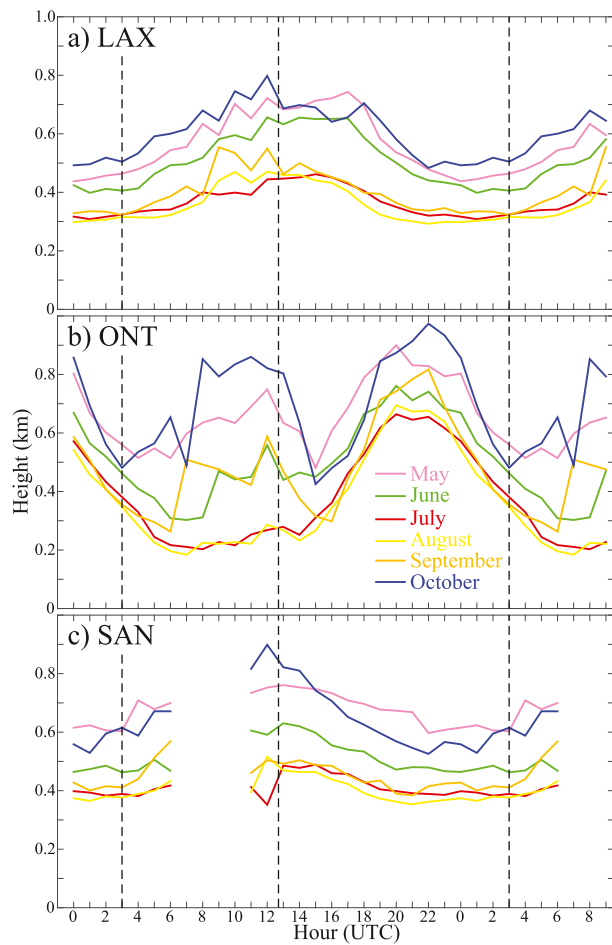


FIG. 7. The diurnal cycle of the average boundary layer depth for (a) LAX, (b) ONT, and (c) SAN. The vertical dashed bars indicate sunrise and sunset on 15 June.

and the cooler months of May, June, and October. For all months, the diurnal range of boundary layer depth averages 45% of the mean value. On a seasonal basis, the average diurnal cycles of boundary layer depth at LAX in July–September are similar to each other, with the lowest boundary layer heights near 380 m and diurnal-variation ranges of 170 m. By contrast, the depth in May, June, and October averages about 580 m, with diurnal variations near 250 m.

#### b. ONT

ONT is inland about 75 km east of LAX and represents a much more continental diurnal signal of the boundary layer (Fig. 8). The elevation of the airport is 280 m, and therefore all reported heights are above ground level. Using all of the observations, a peak in the average boundary layer height of about 780 m is found near 2100 UTC. The minimum occurs some time prior to dawn, but the interquartile range indicates large

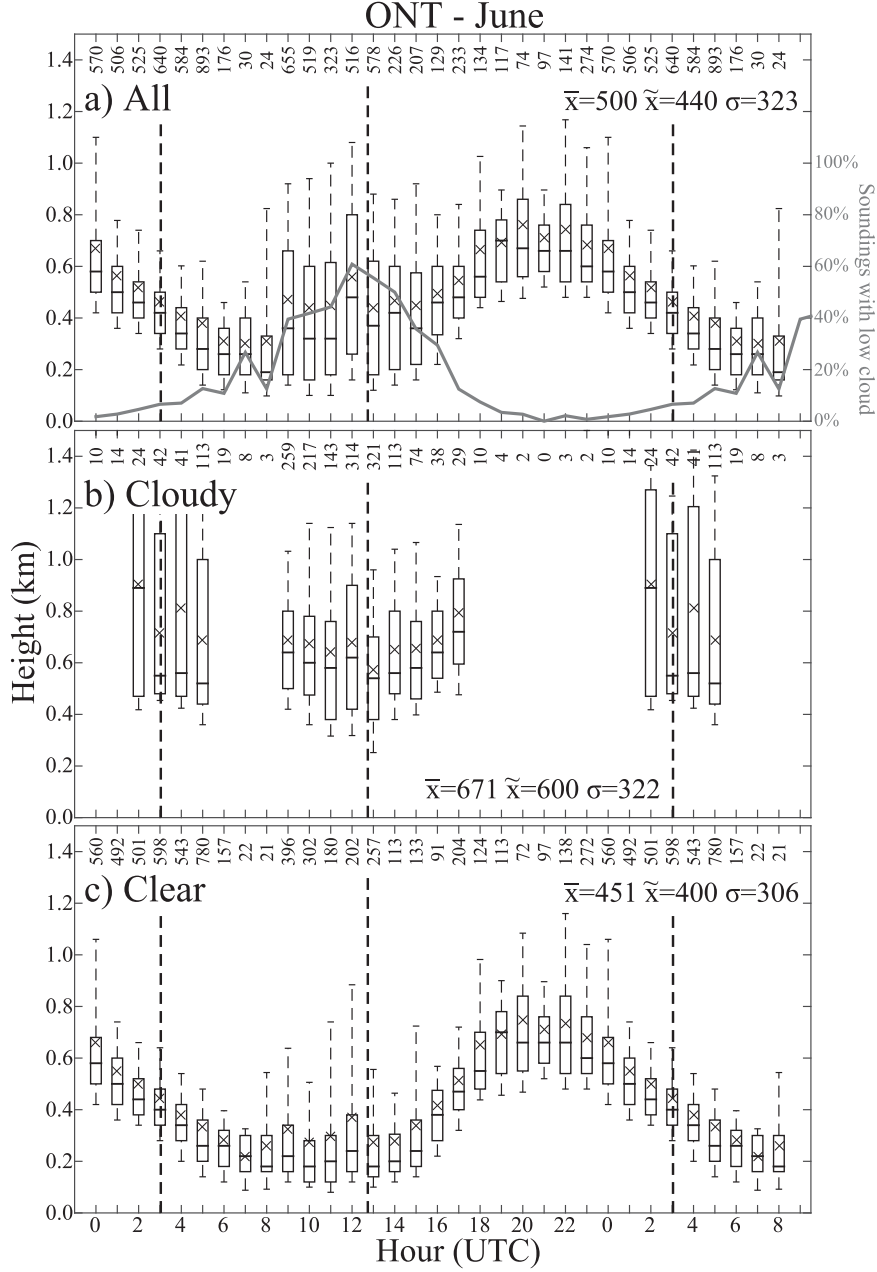


FIG. 8. As in Fig. 6, but for ONT. Note that the elevation of ONT is 280 m and that heights are reported above ground level.

variability beginning at 0900 UTC. If one ignores this variability for the time being, the diurnal signal reflects that of a cloud-free continental location such that the boundary layer growth is dominated by turbulence generated from the surface sensible heating. The interruption of this clean signal indicates that something beyond the local radiational forcing is important. Even though ONT has fewer total observations than LAX, the number of observations in the 0900–1300 UTC timeframe is relatively

high because of the predawn cargo flights of UPS (Fig. 2a). The distribution of the boundary layer height around dawn is greatly skewed toward high heights.

When separating the cloudy and clear soundings, the interpretation becomes more apparent. From 1800 to 0100 UTC there are practically no soundings that are classified as cloudy. From 0900 to 1500 UTC a large portion of the soundings are cloudy and likely represent the nocturnal inland intrusion of the cool marine air,

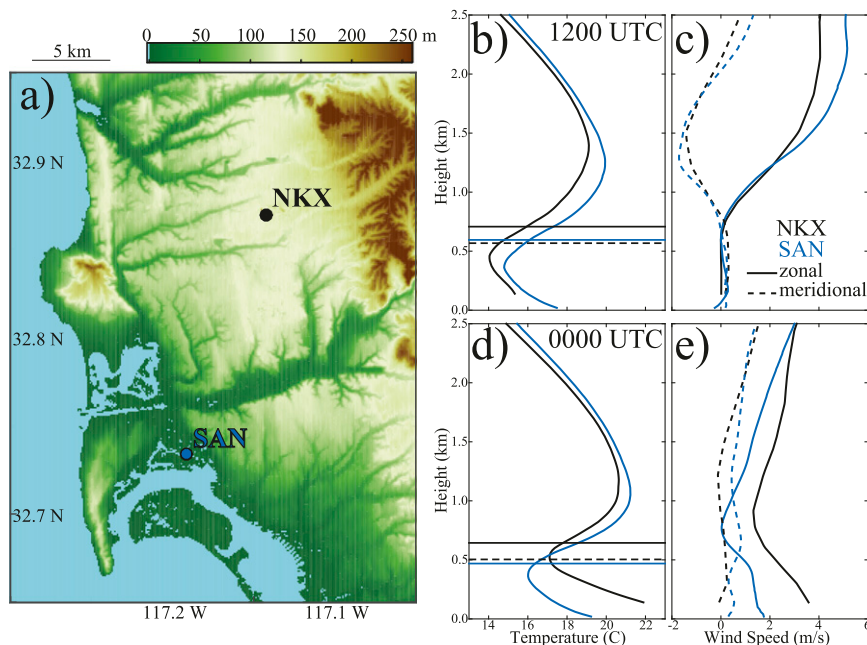


FIG. 9. (a) Elevation map and locations of SAN and NKX. (b) Mean temperature profile ( $^{\circ}\text{C}$ ) using height above sea level for the 1200 UTC soundings for June 2001–14 at SAN (blue) and NKX (black). Horizontal lines indicate mean boundary layer depth, with the dashed line taking into account the elevation difference. (c) Zonal (solid) and meridional (dashed) wind ( $\text{m s}^{-1}$ ). (d),(e) As in (b) and (c), respectively, but at 0000 UTC.

which is often seen in satellite images of stratus encroaching into the Los Angeles basin.

By removing the cloudy soundings, the distribution of hourly boundary layer height becomes narrow and more closely reflects a classic, cloud-free continental diurnal cycle driven by surface heating. The average change of boundary layer depth over the day is 400 m. At 1100 UTC, 45% of the soundings at ONT have been impacted by the intrusion of marine air. These percentages decrease in the hours after sunrise, and practically no influence of the marine air occurs during the afternoon.

Average boundary layer depth for each month during the warm season depicts considerable changes to the diurnal cycle (Fig. 7b). Unlike June, the diurnal cycles during July and August are essentially unaffected by intrusions of marine air that lead to the deeper-than-normal boundary layers in the morning. Except for July and August, every other month exhibits two peaks. The pre-dawn peak is associated with the overnight intrusion of marine air, and the afternoon peak is associated with boundary layer growth promoted by daytime surface heating. The boundary layer average is 670 m in July and August and 880 m otherwise.

### c. SAN

One advantage of SAN is that there are operational radiosondes launched about 15 km to the northeast at

the U.S. Marine Corps Air Station Miramar (NKX), which is at an elevation of 140 m. The operational soundings at NKX allow a comparison between the AMDAR and radiosonde measurements (Fig. 9). Note that the height above sea level is used for the comparison. The mean profiles are the mean of all available data from 2001 to 2014. Similar to what is associated with LAX, most of the AMDAR observations at SAN are taken to the west of the airport into the marine environment. Above the inversion layer, the SAN and NKX temperature profiles are similar as both instruments are measuring the free troposphere, which should be similar over a 15-km horizontal scale. There are obvious differences below the free troposphere that attest to the importance of local processes. It is clear that the boundary layer temperature at SAN has much less diurnal variation than the more inland launch site at NKX. Because SAN is close to the ocean, the temperature remains steady throughout the day. Because NKX is inland and elevated, there is a greater diurnal cycle of temperature within the boundary layer.

Information about the difference in the low-level diurnal cycle of temperature could be obtained by examining the temperature observations from surface stations, but the profiles can provide information about the boundary layer depth and wind profile. The 0000 and 1200 UTC soundings are close to the diurnal minimum and maximum boundary layer depths, respectively (Fig. 10). At 0000 UTC, the

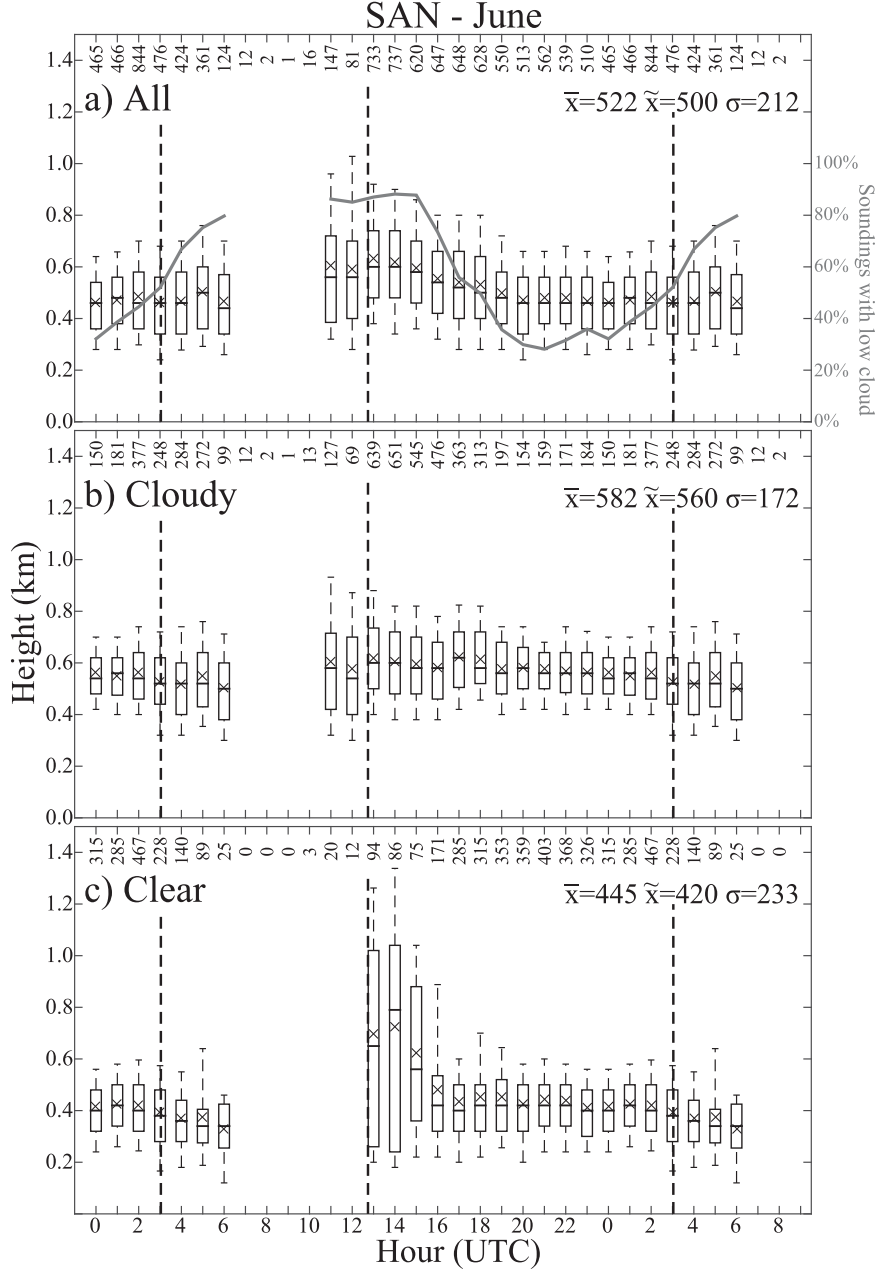


FIG. 10. As in Fig. 6, but for SAN.

boundary layer height at SAN is 470 m but the boundary layer height at NKX is 640 m. Given that NKX is 140 m higher, the average boundary layer depth is 500 m above the surface at NKX. At 1200 UTC, the boundary layer height at SAN is 590 m and at NKX it is 710 m, which is 570 m above the surface. Taking into account the elevation difference, the depth of the boundary layer at both locations is very similar despite the large differences in the boundary layer temperature shown in Fig. 9d.

Good agreement exists between the wind obtained from the radiosondes at NKX and AMDAR observations at SAN. Differences are within about  $0.5 \text{ m s}^{-1}$ . The exception is the zonal wind at 0000 UTC for which the radiosonde at NKX has an approximately  $2 \text{ m s}^{-1}$  greater component than have the SAN measurements. Given the topography around NKX, the difference in zonal wind may have to do with a greater daytime up-slope flow toward the mountains in the east.

Differences between AMDAR at SAN and radiosondes at NKX in this example really stem from differences in the local meteorological conditions. There are two main takeaway points. Differences are small and should give users of AMDAR confidence in the aircraft measurements. The second is that, even though the two airports are just 15 km apart, there can be a noticeable difference in their climatologies. Therefore, any interpretation must take this into account, especially when attempting to use the sounding to characterize the surrounding region. The boundary layer height does agree fairly well when considering the height above the surface.

Returning our attention to the diurnal cycle of boundary layer height at SAN (Fig. 10), the issue of missing data must be addressed. During June from 0700 to 1000 UTC there are only 12, 2, 1, and 16 available AMDAR soundings, respectively. Because there are so few observations, these hours are disregarded when constructing the SAN climatology. The climatology of all of the observed boundary layer heights indicates a maximum just after sunrise at 1300 UTC that drops off throughout the morning and remains low until a couple hours after sunset, when it deepens once more. The interquartile range remains more or less constant, and the distribution is nearly normal. The range of the average diurnal cycle at SAN is 160 m, which is 100 m less than the 260-m range at LAX.

The diurnal cycle of cloudy soundings has only a minor peak in the morning and slightly decreases over the course of the day. Most of the higher heights in the average of all soundings from 1300 to 1500 UTC actually come from the clear soundings. The number of clear soundings in that time frame makes up 12% of the total soundings, but the much higher mean and median heights of the clear soundings drive up the average when using all soundings. The reason for this is unclear and difficult to determine because of the missing data in the hours prior to this morning peak in boundary layer height. Nevertheless, it is noted that, when compared with the cloudy soundings, the clear soundings tend to have stronger offshore flow occurring within the boundary layer from 1300 to 1500 UTC and also from 0400 to 0600 UTC. One conjecture is that the stronger offshore wind could lead to more convergence at the coast and thus increase the boundary layer height. This hypothesis is difficult to test without using other sources of data and numerical simulations.

#### *d. Relation of boundary layer height, wind, and temperature*

The diurnal cycle of temperature at LAX and SAN (Fig. 11) in June reflects nocturnal cooling and deepening of the boundary layer, which is likely driven in part by nocturnal radiative cooling at cloud top because the

majority of soundings overnight are under cloudy conditions. The boundary layer depth obtained through the objective boundary layer detection algorithm is consistent with the diurnal cycle of the temperature profile, confirming the validity of the algorithm. The base of the temperature inversion is located at ~1.2 km. Above 1.6 km there is less diurnal variability.

The time–height cross sections reveal the close relation between the wind and boundary layer height. For each location, the wind components are projected onto the alongshore and cross-shore directions to facilitate the interpretation. The positive alongshore direction at LAX (SAN) is at a compass heading of 295° (345°). The cross-shore component in the boundary layer is clearly dominated by the land and sea breezes at both LAX and SAN. The sea breeze at LAX is about 2 times as strong as the sea breeze at SAN. The land breeze persists until 1500 UTC at both locations. At LAX there is a pronounced offshore flow within the inversion layer overnight.

Overnight, the flow detected by AMDAR reports at LAX is moving toward the northwest with a peak of  $2 \text{ m s}^{-1}$  in the average alongshore wind speed at the top of the boundary layer, a factor that could not have been diagnosed using surface observations alone. This is one clear example in which surface observations inadequately represent the more complete picture of the diurnal cycle given by AMDAR. In June, the low-level cloud in satellite imagery typically reveals cyclonic circulation in the Southern California Bight associated with a recurring Catalina eddy and consistent with the mean alongshore wind at LAX. The average alongshore wind persists until about 1800 UTC and then quickly diminishes into the afternoon. The sudden decrease in the alongshore wind coincides with a rapid drop in the boundary layer height. The alongshore wind at the top of the boundary layer accelerates to the northwest again just after sunset. Even though SAN has missing data before dawn, the alongshore flow is much weaker than what occurs at LAX.

## 4. Conclusions

Two themes were examined: 1) strengths and weaknesses of the AMDAR dataset in constructing a climatology of the lower atmosphere and 2) the creation of a climatology of the lower atmosphere of Southern California. The climatology reveals that AMDAR provides excellent and detailed information when examining the lower atmosphere, even if the information is only tied to the major airports and despite some missing data at certain hours that is due to lack of flights. The high frequency of observations at major airports allows for an unprecedented set of diurnal data at many locations globally.

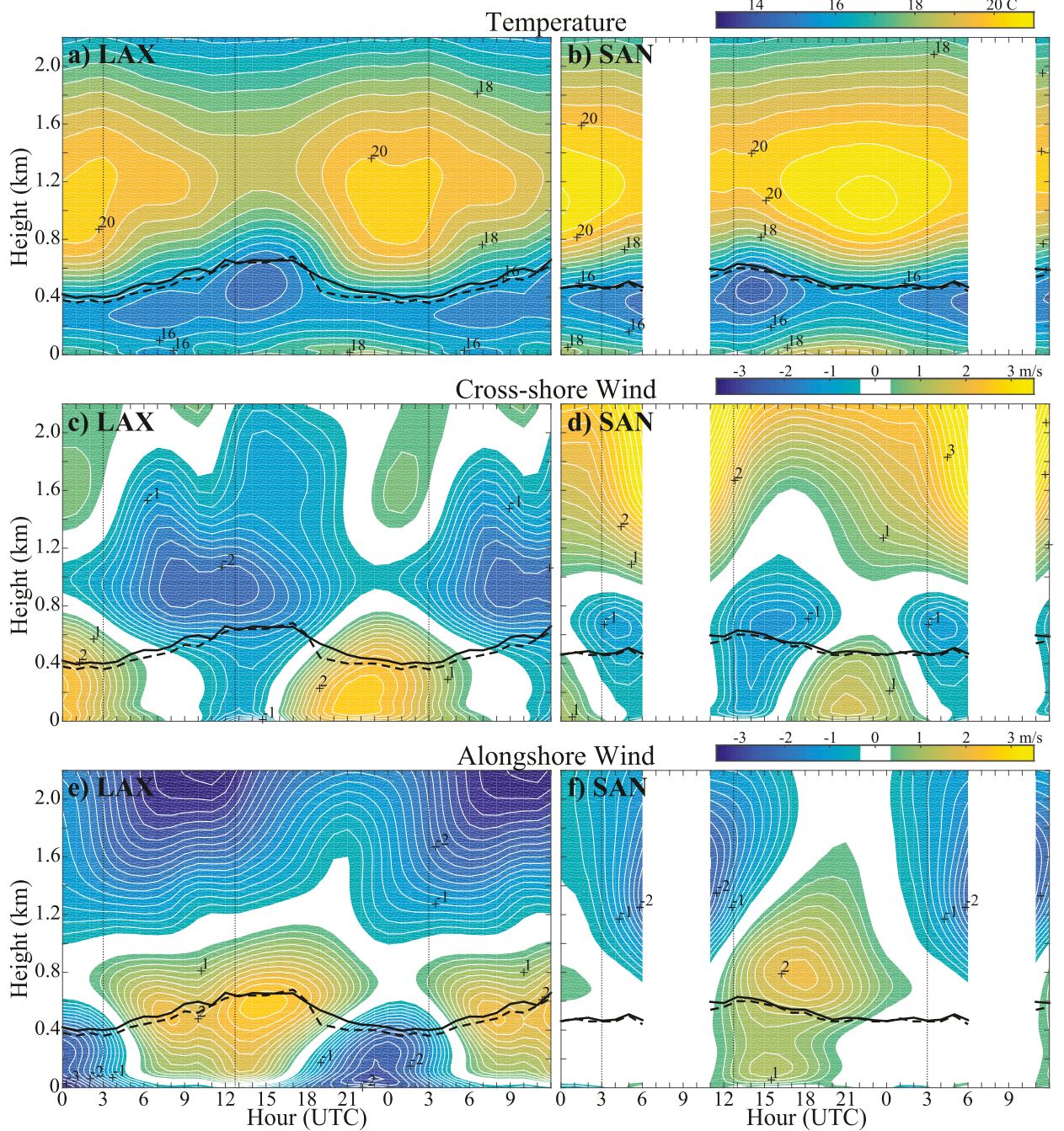


FIG. 11. Time–height cross sections, for (left) LAX and (right) SAN, of the June 2001–14 hourly mean (a),(b) temperature (contoured every  $0.5^{\circ}\text{C}$ ), (c),(d) cross-shore wind (contoured every  $0.2 \text{ m s}^{-1}$ , positive onshore), and (e),(f) alongshore wind (contoured every  $0.2 \text{ m s}^{-1}$ ). The solid (dashed) black line is the mean (median) boundary layer height. The vertical dashed bars indicate sunrise and sunset on 15 June. SAN has missing data between 0700 and 1000 UTC.

The first half of this paper has highlighted several important considerations when constructing a climatology near any airport. Each airport has its own distribution of soundings throughout the day. Airports such as LAX and SAN that mainly serve passenger aircraft have

few, if any, soundings for a few hours before dawn. Conversely, airports such as ONT that mainly serve cargo aircraft may have the most flights in that time period. It is important to recognize that the reported altitude is derived from the standard atmosphere. The

pressure measurement can be backed out, and the hypsometric equation can be used with temperature measurements to obtain a better estimate of the height.

After the initial processing of the soundings, the AMDAR-derived climatology of Southern California was created. The main focus was on June because there is usually an intense temperature inversion that clearly marks the top of the boundary layer. In fact, 88% of the soundings had a clear temperature inversion, as opposed to only 43% in November. At LAX and SAN, there was a deepening of boundary layer depth overnight that is consistent with a cloud-topped boundary layer. At SAN the decrease in boundary layer height begins right after sunrise, but at LAX the deeper boundary layer persists until about 4 h after sunrise and then abruptly decreases as the onshore sea breeze strengthens. Just 75 km east of LAX, ONT is more characteristic of a clear, continental boundary layer driven by surface sensible heat flux with a peak depth late in the afternoon. Morning intrusions of marine air that reach ONT are clearly evident in the monthly average diurnal cycles with the exception of July and August (Fig. 7). Within the inversion layer at LAX there is a clear offshore wind maximum that occurs overnight. The maximum alongshore wind at LAX occurs in the morning at the top of the boundary layer and is associated with the common cyclonic circulation seen in satellite images. The diurnal variation of boundary layer depth at LAX is larger than at SAN, suggesting an alongshore pressure gradient force that also varies diurnally.

The quality and large number of soundings contained in the AMDAR dataset contribute to long-term monitoring of the lower atmosphere in a fairly cost-effective way when compared with radiosonde measurements (e.g., Petersen 2016). The major advantage over radiosondes is the greater amount of sampling, despite the small temperature bias in AMDAR measurements near the surface. Although AMDAR data have been primarily used for data assimilation and short-term forecasting, this dataset is also valuable when used to construct climatologies. In this work, we present the baseline climatology of three airports in the California Bight, which by itself is of interest, but we also believe that AMDAR may be employed for a variety of more specific applications. For instance, the development of Catalina eddies might be better quantified by examining the departure from the climatology during days with pronounced Catalina eddies.

**Acknowledgments.** This research was supported in part by NFGRF-2302312 and the National Science Foundation through Grant AGS-1439515. We thank Randy Baker for his valuable experience and insight regarding the use of AMDAR data and David Braaten

and David Mechem for helpful discussions. We also thank the three anonymous reviewers for their insight and helpful suggestions.

## REFERENCES

- Angevine, W. M., L. Eddington, K. Durkee, C. Fairall, L. Bianco, and J. Brioude, 2012: Meteorological model evaluation for CalNex 2010. *Mon. Wea. Rev.*, **140**, 3885–3906, doi:[10.1175/MWR-D-12-00042.1](https://doi.org/10.1175/MWR-D-12-00042.1).
- Ballish, B. A., and V. K. Kumar, 2008: Systematic differences in aircraft and radiosonde temperatures: Implications for NWP and climate studies. *Bull. Amer. Meteor. Soc.*, **89**, 1689–1707, doi:[10.1175/2008BAMS2332.1](https://doi.org/10.1175/2008BAMS2332.1).
- Blaskovic, M., R. Davies, and J. B. Snider, 1991: Diurnal variation of marine stratocumulus over San Nicolas Island during July 1987. *Mon. Wea. Rev.*, **119**, 1469–1478, doi:[10.1175/1520-0493\(1991\)119<1469:DVOMSO>2.0.CO;2](https://doi.org/10.1175/1520-0493(1991)119<1469:DVOMSO>2.0.CO;2).
- Bosart, L. F., 1983: Analysis of a California Catalina eddy. *Mon. Wea. Rev.*, **111**, 1619–1633, doi:[10.1175/1520-0493\(1983\)111<1619:AOACCE>2.0.CO;2](https://doi.org/10.1175/1520-0493(1983)111<1619:AOACCE>2.0.CO;2).
- Brooks, I. M., A. K. Goroch, and D. P. Rogers, 1999: Observations of strong surface radar ducts over the Persian Gulf. *J. Appl. Meteor.*, **38**, 1293–1310, doi:[10.1175/1520-0450\(1999\)038<1293:OOSSRD>2.0.CO;2](https://doi.org/10.1175/1520-0450(1999)038<1293:OOSSRD>2.0.CO;2).
- Burk, S. D., and W. T. Thompson, 1997: Mesoscale modeling of summertime refractive conditions in the Southern California Bight. *J. Appl. Meteor.*, **36**, 22–31, doi:[10.1175/1520-0450\(1997\)036<0022:MMOSRC>2.0.CO;2](https://doi.org/10.1175/1520-0450(1997)036<0022:MMOSRC>2.0.CO;2).
- Cardinali, C., L. Isaksen, and E. Andersson, 2003: Use and impact of automated aircraft data in a global 4DVAR data assimilation system. *Mon. Wea. Rev.*, **131**, 1865–1877, doi:[10.1175/2569.1](https://doi.org/10.1175/2569.1).
- de Szoete, S. P., S. Yuter, D. Mechem, C. W. Fairall, C. D. Burleyson, and P. Zuidema, 2012: Observations of stratocumulus clouds and their effect on the eastern Pacific surface heat budget along 20°S. *J. Climate*, **25**, 8542–8567, doi:[10.1175/JCLI-D-11-00618.1](https://doi.org/10.1175/JCLI-D-11-00618.1).
- Gao, F., X. Zhang, N. A. Jacobs, X. Huang, X. Zhang, and P. P. Childs, 2012: Estimation of TAMDAR observational error and assimilation experiments. *Wea. Forecasting*, **27**, 856–877, doi:[10.1175/WAF-D-11-00120.1](https://doi.org/10.1175/WAF-D-11-00120.1).
- Haack, T., and S. T. Burk, 2001: Summertime marine refractivity conditions along coastal California. *J. Appl. Meteor.*, **40**, 673–687, doi:[10.1175/1520-0450\(2001\)040<0673:SMRCAC>2.0.CO;2](https://doi.org/10.1175/1520-0450(2001)040<0673:SMRCAC>2.0.CO;2).
- Hu, X.-M., J. W. Nielsen-Gammon, and F. Zhang, 2010: Evaluation of three planetary boundary layer schemes in the WRF Model. *J. Appl. Meteor. Climatol.*, **49**, 1831–1844, doi:[10.1175/2010JAMC2432.1](https://doi.org/10.1175/2010JAMC2432.1).
- Isaksen, L., D. Vasiljevic, R. Dee, and S. Healy, 2011: Bias correction of aircraft data. *ECMWF Newsletter*, No. 131, ECMWF, Reading, United Kingdom, 6. [Available online at <http://www.ecmwf.int/sites/default/files/elibrary/2012/14591-newsletter-no131-spring-2012.pdf>.]
- LeMone, M. A., M. Tewari, F. Chen, and J. Dudhia, 2014: Objectively determined fair-weather NBL features in ARW-WRF and their comparison to CASES-97 observations. *Mon. Wea. Rev.*, **142**, 2709–2732, doi:[10.1175/MWR-D-13-00358.1](https://doi.org/10.1175/MWR-D-13-00358.1).
- Lilly, D., 1968: Models of cloud-topped mixed layers under a strong inversion. *Quart. J. Roy. Meteor. Soc.*, **94**, 292–309, doi:[10.1002/qj.49709440106](https://doi.org/10.1002/qj.49709440106).
- Lord, R. J., W. P. Menzel, and L. E. Pecht, 1984: ACARS wind measurements: An intercomparison with radiosonde, cloud

- motion, and VAS thermally derived winds. *J. Atmos. Oceanic Technol.*, **1**, 131–137, doi:[10.1175/1520-0426\(1984\)001<0131:AWMAIW>2.0.CO;2](https://doi.org/10.1175/1520-0426(1984)001<0131:AWMAIW>2.0.CO;2).
- Mass, C. F., and M. D. Albright, 1989: Origin of the Catalina eddy. *Mon. Wea. Rev.*, **117**, 2406–2436, doi:[10.1175/1520-0493\(1989\)117<2406:OOTCE>2.0.CO;2](https://doi.org/10.1175/1520-0493(1989)117<2406:OOTCE>2.0.CO;2).
- Moninger, W. R., R. D. Mamrosh, and P. M. Pauley, 2003: Automated meteorological reports from commercial aircraft. *Bull. Amer. Meteor. Soc.*, **84**, 203–216, doi:[10.1175/BAMS-84-2-203](https://doi.org/10.1175/BAMS-84-2-203).
- NOAA, 2014: Termination of continental United States wind profiler observation data on or about August 30, 2014. National Oceanic and Atmospheric Administration Service Change Notice (SCN) 14-36. [Available online at [http://www.nws.noaa.gov/om/notification/scn14-36wind\\_profilers.htm](http://www.nws.noaa.gov/om/notification/scn14-36wind_profilers.htm).]
- Petersen, R., 2016: On the impact and benefits of AMDAR observations in operational forecasting. Part I: A review of the impact of automated aircraft wind and temperature reports. *Bull. Amer. Meteor. Soc.*, **97**, 585–602, doi:[10.1175/BAMS-D-14-00055.1](https://doi.org/10.1175/BAMS-D-14-00055.1).
- Rahn, D. A., T. R. Parish, and D. Leon, 2013: Airborne measurements of coastal jet transition around Point Conception, California. *Mon. Wea. Rev.*, **141**, 3827–3839, doi:[10.1175/MWR-D-13-00030.1](https://doi.org/10.1175/MWR-D-13-00030.1).
- Rogers, D. P., and Coauthors, 1998: Highlights of Coastal Waves 1996. *Bull. Amer. Meteor. Soc.*, **79**, 1307–1326, doi:[10.1175/1520-0477\(1998\)079<1307:HOCW>2.0.CO;2](https://doi.org/10.1175/1520-0477(1998)079<1307:HOCW>2.0.CO;2).
- Rosenthal, J., 1968: A Catalina eddy. *Mon. Wea. Rev.*, **96**, 742–743, doi:[10.1175/1520-0493\(1968\)096<0742:ACE>2.0.CO;2](https://doi.org/10.1175/1520-0493(1968)096<0742:ACE>2.0.CO;2).
- Stevens, B., and Coauthors, 2003: Dynamics and Chemistry of Maritime Stratocumulus—DYCOMS-II. *Bull. Amer. Meteor. Soc.*, **84**, 579–593, doi:[10.1175/BAMS-84-5-579](https://doi.org/10.1175/BAMS-84-5-579).
- Wakimoto, R., 1987: The Catalina eddy and its effect on pollution in Southern California. *Mon. Wea. Rev.*, **115**, 837–855, doi:[10.1175/1520-0493\(1987\)115<0837:TCEAIE>2.0.CO;2](https://doi.org/10.1175/1520-0493(1987)115<0837:TCEAIE>2.0.CO;2).
- Wang, C., D. Wilson, T. Haack, P. Clark, H. Lean, and R. Marshall, 2012: Effects of initial and boundary conditions of mesoscale models on simulated atmospheric refractivity. *J. Appl. Meteor. Climatol.*, **51**, 115–132, doi:[10.1175/JAMC-D-11-012.1](https://doi.org/10.1175/JAMC-D-11-012.1).
- WMO, 2014a: Requirements for the implementation and operation of an AMDAR programme. World Meteorological Organization Integrated Observing System Tech. Rep. 2014-2, 28 pp. [Available online at [ftp://ftp.wmo.int/Documents/www/amdar/documents/wigos-tr\\_2014-02\\_en.pdf](ftp://ftp.wmo.int/Documents/www/amdar/documents/wigos-tr_2014-02_en.pdf).]
- , 2014b: The benefits of AMDAR to meteorology and aviation. World Meteorological Organization Integrated Observing System Tech. Rep. 2014-1, 47 pp. [Available online at [ftp://ftp.wmo.int/Documents/www/amdar/documents/wigos-tr\\_2014-01\\_en.pdf](ftp://ftp.wmo.int/Documents/www/amdar/documents/wigos-tr_2014-01_en.pdf).]
- Zhu, Y., J. Derber, R. J. Purser, J. Whiting, and B. R. Ballish, 2015: Variational correction of aircraft temperature bias in the NCEP's GSI analysis system. *Mon. Wea. Rev.*, **143**, 3774–3803, doi:[10.1175/MWR-D-14-00235.1](https://doi.org/10.1175/MWR-D-14-00235.1).